Integrating Graph Neural Networks and Many-Body Expansion Theory for Potential Energy Surfaces

Siqi Chen[1,*] **Zhiqiang Wang**[1,2,*] **Xianqi Deng**[1,3,*] **Yili Shen**[1,4,*] **Cheng-Wei Ju**[1,5]
Jun Yi[1,6] **Lin Xiong**[1] **Guo Ling**[1] **Dieaa Alhmoud**[1] **Hui Guan**[1,†] **Zhou Lin**[1,†]
[1]University of Massachusetts Amherst [2]Florida Atlantic University [3]University at Albany
[4]University of Notre Dame [5]The University of Chicago [6]Wake Forest University
[*]These authors contribute equally to this study.
[†]Corresponding authors: {huiguan,zhoulin}@umass.edu

Abstract

Rational design of next-generation functional materials relied on quantitative predictions of their electronic structures beyond single building blocks. First-principles quantum mechanical (QM) modeling became infeasible as the size of a material grew beyond hundreds of atoms. In this study, we developed a new computational tool integrating fragment-based graph neural networks (FBGNN) into the fragment-based many-body expansion (MBE) theory, referred to as FBGNN-MBE, and demonstrated its capacity to reproduce full-dimensional potential energy surfaces (FD-PES) for hierarchic chemical systems with manageable accuracy, complexity, and interpretability. In particular, we divided the entire system into basic building blocks (fragments), evaluated their single-fragment energies using a first-principles QM model and attacked many-fragment interactions using the structure–property relationships trained by FBGNNs. Our development of FBGNN-MBE demonstrated the potential of a new framework integrating deep learning models into fragment-based QM methods, and marked a significant step towards computationally aided design of large functional materials.

1 Introduction

Discovery of complex materials that exhibited exceptional quantum mechanical (QM) properties and function beyond single monomers and equilibrium structures, such as metal–organic frameworks (MOF) [1], organic semiconductors (OSC) [2], and branched deoxyribonucleic acids (DNA) [3], was crucial in emergent scientific and technological areas, such as carbon neutrality [4], renewable energy [5], and next-generation optoelectronics [6]. Computational chemistry eliminated expensive trial-and-error experiments and explored the vast chemical space. In the present study, we aimed to accomplish a computational design for these complex materials based on their aggregate and dynamic QM properties, which required a rapid and rigorous evaluation of their full-dimensional potential energy surfaces (FD-PES) on the fly. This job cannot be done by first-principles QM models like second-order Møller–Plesset perturbation theory (MP2) [7] or density functional theory (DFT) [8, 9] due to the prohibitive costs for large systems because their computational complexity scaled as the fifth and third power of the number of basis functions [10, 11].

Motivated by this problem, many fragment-based "divide-and-conquer" methods were developed to accelerate typical QM approaches while maintaining the accuracy [12, 13]. Among all these theories, many-body expansion (MBE) stood out due to its straightforward implementation and rapid convergence for many-body interactions [14–16]. MBE partitioned a complex system into manageable fragments (bodies) and expanded the total electronic energy or other relevant properties into a series of one-body (1B) and many-body (nB) terms with progressively diminishing contributions. This

38th Conference on Neural Information Processing Systems (NeurIPS 2024).

hierarchical treatment not only streamlined a calculation with a reduced computational complexity but also enabled a deeper analysis of the electronic structure landscape and the intricate many-fragment interactions, both of which were critical properties for computational material discovery.

The Herbert group and the Xantheas group made prominent and complementary contributions in recent methodology of MBE for both static and dynamic behaviors of condensed-phase systems. Herbert and coworkers developed the generalized many-body expansion (GMBE) framework to handle systems with ill-defined or overlapping fragments like fluoride-water complexes. They also introduced energy-screened MBE with enhanced efficiency and intact accuracy by selectively including only sizable many-body contributions in the total electronic energy [15, 17–25]. Xantheas and coworkers leveraged MBE for potential energy surfaces (PES) and demonstrated that MBE can provide a more quantitative understanding of molecular properties than simpler pairwise-additive models. They further incorporated MBE into molecular dynamics (MD) simulations to involve subtle QM phenomena for electrons and nuclei [16, 26–36]. Despite these advances, applying QM-based MBE to functional materials with more sophisticated structures and more intense interactions than water clusters remains a challenge due to the large numbers of n-fragment interactions for high n's.

The integration of neural networks (NNs) offered a revolutionary approach to accelerate QM methods like MBE [37–39]. In particular, Parkhill and coworkers merged NN into MBE (NN-MBE) and demonstrated its strong predictive power for the FD-PES of methanol (CH_3OH) clusters with mean absolute errors (MAEs) of 9.79 and 12.55 kcal/mol for two-body (2B) and three-body (3B) energies compared to MP2 but a reduced computational cost by six orders of magnitude [40]. However, intrinsic problems of traditional NNs in terms of the missing physical information [37, 41], the limited transferability and interpretability [42, 43], and inability to handle graph-structured data [44, 45] compromised their capacity in QM modeling [46, 47].

Instead, the development of graph neural networks (GNNs) experienced exceptional success in chemical systems because their node–edge structures naturally aligned with three-dimensional atom–bond structures and encoded mechanical information about chemical bonds and intermolecular interactions [44, 45, 48–50]. Outstanding examples included SchNet [51], GeoMol [52], FP-GNN (fingerprints-GNN) [53], and dyMEAN (dynamic multi-channel equivariant graph network) [54] which incorporated complex geometric information in the graph representation, PhysNet [55], DimeNet/DimeNet++ (directional message passing NN) [56, 57], E(n) EGNN (equivariant GNN) [58], SEGNN (steerable E(3) equivariant GNN) [59], and ViSNet (vector-scalar interactive GNN) [60] which integrated directional message passing framework and physical principles, and ml-QM-GNN (QM-augmented GNN) [61], MD-GNN (mechanism-data-driven graph neural network) [62], MP-GNN (multiphysical GNN) [63], and SS-GNN (simple-structured graph neural network) [64] which implemented quantitative mechanical and electronic properties. Most of these GNN models demonstrated enhanced performance in molecular representation learning but they treated all atoms on equal footing without considering the chemical hierarchy, which impacted their descriptive and predictive capacity for complex systems with many building blocks.

State-of-the-art GNN models with subgraph of fragment-based frameworks, such as SubGNN (subgraph NN) [65], FragGraph [66], subGE (subgraph embedding) [67], MXMNet (multiplex molecular GNN) [68], and PAMNet (physics aware multiplex GNN) [69], all represented building blocks like molecules or monomers into subgraphs or local graphs, and captured interatomic, intermolecular and interfragment interactions using local and global message-passing architectures. Such an analogy between hierarchic graph structures and hierarchic chemical systems rendered these models outstanding methods for studying complex systems. In particular, MXMNet and PAMNet developed by Xie and coworkers significantly advanced the representation learning of hierarchic systems by integrating molecular mechanics and multiplex graph representations and proved successful in reproducing the molecular properties from the QM9 data set [70], the protein–ligand binding affinities from the PDBBind data set [71], and the three-dimensional (3D) structures of ribonucleic acids (RNA) [72].

In the present study, we developed a novel computational model named FBGNN-MBE (fragment-based graph neural network driven many-body expansion) to address all problems mentioned above. Our ultimate goal was to accomplish a rapid, precise, transferable, and interpretable scheme to evaluate FD-PES for any functional materials with many building blocks and important dynamic properties. Our major contributions include:

- We established FBGNN-MBE to integrate the divide-and-conquer strategy of the MBE formalism with the sophisticated modeling capacity of FBGNN.

- We attacked the total ground state electronic energy using MBE and expected an extension to excited state energies and other properties.
- We evaluated 1B energies using MP2 or DFT and generated 2B and 3B energies based on 3D atomistic geometries and structure–property relationships trained by MXMNet or PAMNet.
- We provided a proof-of-concept for FBGNN-MBE using three benchmark systems with weak to moderate many-fragment interactions.
- We arrived at chemical accuracy (< 0.3 kcal/mol) for 2B and 3B energies across all systems and outperformed other MBE models using conventional GNNs.
- We interpreted the outstanding performance of FBGNN-MBE through the natures and strengths of many-fragment interactions in benchmark systems.
- We designed application systems to evaluate FBGNN-MBE in reproducing experimental measurable properties based on FD-PES.
- We confirmed the potential of FBGNN-MBE as a revolutionary protocol for computational material discovery.

2 Methods

2.1 Many-Body Expansion Theory

MBE decomposed any aggregate property, such as the total ground state energy (E), into contributions from individual fragments (1B) and many-fragment (nB) interactions. Truncated at a vanishing high-order term, MBE facilitated an efficient approximation of the property in question. Beyond reducing the computational cost, MBE also enabled the capture of the natures and strengths of many-fragment interactions in a chemical system. The generic MBE theory partitioned a system into N fragments and expands E until the a higher order tuncation (3 here) [16]:

$$E = \sum_{i}^{N} E_i^{\mathrm{1B}} + \sum_{i<j}^{N} E_{ij}^{\mathrm{2B}} + \sum_{i<j<k}^{N} E_{ijk}^{\mathrm{3B}} \tag{1}$$

E_i^{1B} represented a 1B energy for the isolated i^{th} fragment. E_{ij}^{2B} represented a 2B energy, capturing the interactions between the i^{th} and j^{th} fragments. E_{ijk}^{3B} represented a 3B energy, providing more complicated interactions among the i^{th}, j^{th}, and k^{th} fragments. As such

$$E_i^{\mathrm{1B}} = E_i \tag{2}$$

$$E_{ij}^{\mathrm{2B}} = E_{ij} - E_i^{\mathrm{1B}} - E_j^{\mathrm{1B}} \tag{3}$$

$$E_{ijk}^{\mathrm{3B}} = E_{ijk} - E_{ij}^{\mathrm{2B}} - E_{ik}^{\mathrm{2B}} - E_{jk}^{\mathrm{2B}} - E_i^{\mathrm{1B}} - E_j^{\mathrm{1B}} - E_k^{\mathrm{1B}} \tag{4}$$

Although higher-order terms captured more complex interactions, we neglected beyond 3B energies due to vanishing contributions, tolerable errors, and exponentially-growing sizes. We discussed our fragmentation strategies in Section A.2. In FBGNN-MBE, we utilized a hybrid strategy by calculating 1B energies using MP2 or DFT but leveraging FBGNNs for 2B and 3B energies (Figure 1).

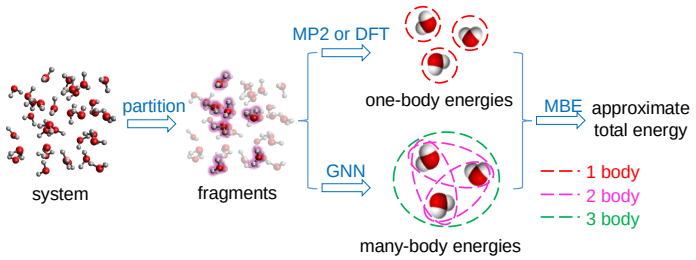

Figure 1: Schematic strategy of our FBGNN-MBE approach integrating FBGNNs into the MBE theory, using a water cluster as an illustrative example.

2.2 Fragment-Based Graph Neural Networks

General Architecture of GNNs A GNN typically employed multiple convolution layers to transform input features into node embeddings, followed by graph pooling to generate a graph representa-

tion, which can then be used for various downstream tasks such as predicting 2B and 3B energies [44, 45, 73]. In chemical applications, the input graph was structured with features, including nodes representing individual atoms and edges capturing pairwise interatomic interactions as functions of atomistic structures. Each node was initialized with features that described its atomic properties, such as atomic number, charge, electronegativity, and even orbitals, while each edge reflected an interatomic distance or a bond length. These features iteratively updated the node embeddings by aggregating information from neighboring nodes and effectively extract the local environment each atom resided in.

Backbone MXMNet and PAMNet Models We employed MXMNet [68] and PAMNet [69] as our backbone FBGNN models. Building on the general GNN framework, MXMNet and PAMNet leveraged multiplex global–local architectures to align with hierarchic chemical systems. They represented the entire material as the global graph ($\mathcal{G}_\mathrm{g}$) and every single building block as a local graph ($\mathcal{G}_\mathrm{l}$, or subgraph). They also represented short-range interatomic interactions as local edges ($\mathcal{E}_\mathrm{l}$) within a local graph, and long-range interfragment interactions as global edges ($\mathcal{E}_\mathrm{g}$) between local graphs. Both models applied a two-layer multiplex graph ($\mathcal{G} = \mathcal{G}_\mathrm{g}, \mathcal{G}_\mathrm{l}$). The global graph viewed the entire system as a network of pre-defined fragments (local graphs) and many-fragment interactions (global edges), symbolized as $\mathcal{G}_\mathrm{g} = (\mathcal{G}_\mathrm{l}, \mathcal{E}_\mathrm{g})$. Each local graph, containing a single fragment, viewed this fragment as a network of atoms [nodes ($\mathcal{V}$)] and chemical bonds (local edges), symbolized as $\mathcal{G}_\mathrm{l} = (\mathcal{V}, \mathcal{E}_\mathrm{l})$. The cross mapping modules and the message passing algorithms [42] integrated all information from the global and local layers (Figure 2). This scheme allowed us to implement the geometric information about a chemical system directly into the global and local graph representations for downstream tasks and to seamlessly connect to the next-stage model design to further refine and process these models.

The architecture of MXMNet included three modules (Figure 2 in burgundy boxes). The embedding module converted the Coulomb matrix [74], which contained atomic charges and interatomic distances, into a trainable embedding vector as the initial node feature for the multiplex graph. The multiplex molecular (MXM) module incorporated the local message passing mechanism, the global message passing mechanism [42], and the cross layer mapping for interactively updating node embeddings and local graph representation, and was the foundational component in the multiplex molecular graphs. The prediction module leveraged the final node embeddings to predict fragment-specific and system-wide properties in question [68]. An overall heterogeneous structure like this proved superior to conventional GNNs [75, 76]. Building upon MXMNet, PAMNet implemented an additional fusion module to integrate different types of interactions into the final prediction while ensuring the E(3)-invariance of the presentations (Figure 2 in orange boxes). This fusion model not only enhanced the model accuracy and efficiency in capturing key features from geometric and electronic structures but also simplified the process [69]. Given the complexity of the data structure, we utilized the Adam optimizer [77]for faster convergence and higher suitability for complex systems. We provided the pseudo-algorithms of MXMNet and PAMNet in the context of MBE in Section A.1.

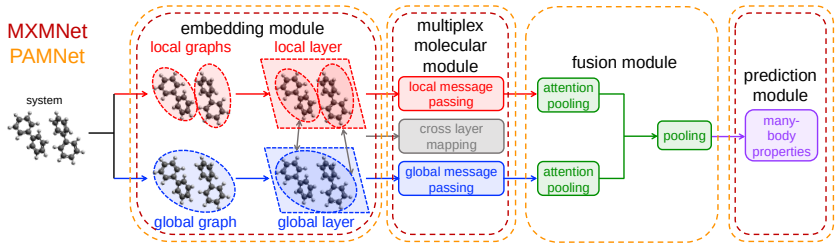

Figure 2: Schematic design of MXMNet (burgundy boxes) and PAMNet (orange boxes) for a multi-fragment complex system [68, 69].

3 Experiments

3.1 Benchmark Systems

To provide a proof-of-concept of our MXMNet-MBE and PAMNet-MBE models and assess their robustness, accuracy, and efficiency to reproduce 2B and 3B interactions, we established benchmark

systems with three molecular clusters whose structures and behaviors depended on weak or moderate interactions between building blocks, including pure water (H_2O) with moderate or strong hydrogen bonds, pure phenol (C_6H_5OH) with weak hydrogen bonds and van der Waals interactions, and a 1:1 water–phenol (H_2O:C_6H_5OH) mixture showing a synergistic effect of the two interactions [78, 79]. We carved all systems from condensed phases, and designed every single water or phenol molecule as a single fragment, and collected all possible dimers and trimers for the evaluation of 2B and 3B energies in Equation (1). We calculated 1B energies using DFT or MP2 and predicted 2B and 3B energies using MXMNet and PAMNet models.

3.2 Molecular Dynamics and Quantum Mechanical Calculations.

Table 1: Summary of Molecular Dynamics Details

Data Set	Molecules	T (K)	Dimers	Trimers	t_{em} (ns)	t_{eq} (ns)	t_{pr} (ns)
H_2O	67	370	48,643	1,053,911	0.5	0.1	2.0
C_6H_5OH	10	360	45,045	120,120	0.5	0.1	1.0
H_2O:C_6H_5OH	10:10	694	190,000	228,000	0.5	0.1	0.1

To sample an ergodic and sufficient data set for each benchmark system, we included high-energy points from its FD-PES. We employed MD simulations at the canonical ensemble (constant NVT) using GROMACS [80] at a doubled ($2\times$) density, and generated their initial configurations using PACKMOL [81]. We also set temperatures close to or above the boiling point to ensure a faster equilibration. For each simulation we performed energy minimization (t_{em}), equilibration (t_{eq}), and production (t_{pr}), and collected a large number of snapshots. We summarized all the details of our MD simulations in Table 1. From each snapshot, we collected all dimers and trimers to create a data set with a broad representation of geometric configurations and interfragment interactions. For each data set, we randomly split them into an 80:5:15 ratio for training, validation, and test sets. To establish the training set and calibrate the validation and test sets, we calculated all monomer, dimer, and trimer energies using QM methods, which were MP2 [7, 82] with the aug-cc-pVDZ basis set [83, 84] for water clusters and DFT with the ωB97X-D3 exchange–correlation functional [85] and the 6-311+G(d,p) basis set for phenol-involving clusters [86], all in Q-Chem 6.2 [87]. Following the QM calculations, we calculateed 2B and 3B energies (E_{ij}^{2B} and E_{ijk}^{3B}) as outlined in Equations (3) and (4).

3.3 Inputs and Outputs

The input structure of our data sets was comprised of atom types (*e.g.*, O, H, C), 3D atomic coordinates to capture spatial relationships, and calculated 1B, 2B and 3B energies for all possible monomers, dimers, and trimers. The output structure was comprised of FBGNN-predicted 2B and 3B energies for these configurations.

3.4 Hyperparameter Tuning

Hyperparameter tuning was executed using the validation set for each benchmark system [88]. We identified six critical hyperparameters: the number of epochs (N_{epoch}), the number of convolutional layers (N_{layer}), the local cutoff distance (D_{lc}), the global cutoff distance (D_{gc}), the batch size (N_{batch}), and the learning rate (k_{learn}), because they demonstrated significant impact on GNN performance in molecular modeling [89]. During this process we evaluated the model performance after each epoch by monitoring the validation loss and employed an early stopping mechanism to prevent overfitting.

4 Results and Discussions

To confirm the potential of FBGNN-MBE models in reproducing FD-PES for functional materials, we exhibited their state-of-the-art performance in predicting 2B and 3B energies for all three benchmark systems. In Figures 3 and 4, we compared 2B and 3B energies evaluated using MP2 or DFT with their counterparts predicted by MXMNet-MBE and PAMNet-MBE. We also summarized their values of R-squared coefficient (R^2), mean signed errors (MSE), MAE, and average CPU/GPU times for first-principles (FP) and GNN treatments in Table 2, with their definitions in the Section A.4.

Table 2: Comparative Performance of MXMNet-MBE and PAMNet-MBE Models

Model	Dataset	R^2	$\langle E_{\text{FP}} \rangle$	MSE	MAE	$\langle t_{\text{FP}} \rangle$	$\langle t_{\text{GNN}} \rangle$
			kcal/mol			s	
MXMNet	H_2O 2B	0.9400	+0.2550	+0.0015	0.2604	1.29	0.09
	H_2O 3B	0.9998	−0.0008	+0.0005	0.0121	2.97	0.08
	C_6H_5OH 2B	0.9955	+1.1199	−0.0002	0.1483	147.51	8.83
	C_6H_5OH 3B	0.8704	+0.0010	+0.0007	0.0522	428.17	3.94
	H_2O:C_6H_5OH 2B	0.9980	+0.8180	−0.0023	0.0684	69.77	4.67
	H_2O:C_6H_5OH 3B	0.8421	−0.0088	0.0000	0.0355	198.77	3.98
PAMNet	H_2O 2B	0.9230	+0.2550	+0.0021	0.2766	1.29	0.11
	H_2O 3B	0.9999	−0.0008	+0.0015	0.0109	2.97	0.07
	C_6H_5OH 2B	0.9963	+1.1199	−0.0075	0.1348	147.51	8.88
	C_6H_5OH 3B	0.8772	+0.0010	+0.0007	0.0526	428.17	3.35
	H_2O:C_6H_5OH 2B	0.9982	+0.8180	−0.0024	0.0654	69.77	4.68
	H_2O:C_6H_5OH 3B	0.8515	−0.0088	+0.0001	0.0353	198.77	3.76

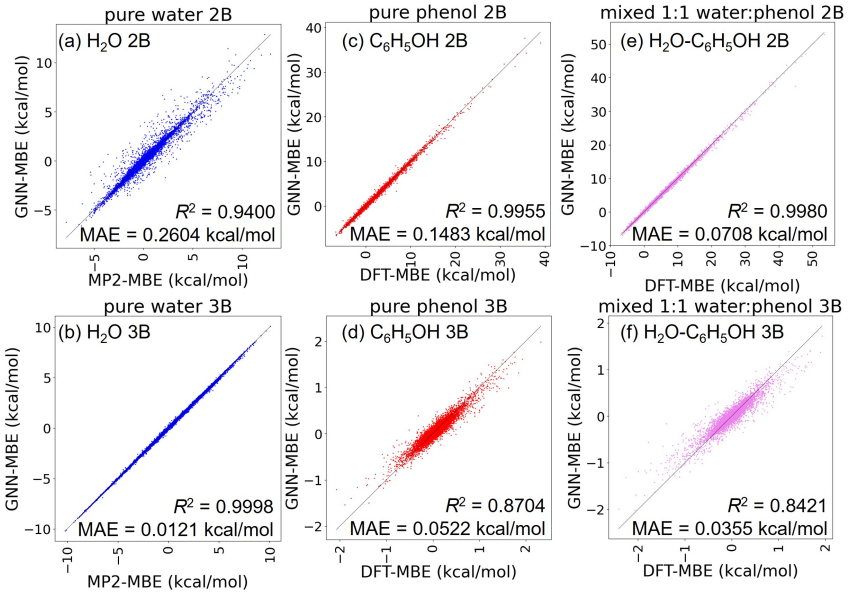

Figure 3: Comparison between MXMNet-predicted and MP2/DFT-evaluated 2B and 3B energies for all three benchmark systems.

4.1 Overall Performance Assessment

We herein analyzed the overall performance of MXMNet-MBE and PAMNet-MBE to provide a proof-of-concept for these two models using benchmark systems. In the tasks of predicting 2B and 3B energies, both MXMNet-MBE and PAMNet-MBE demonstrated extremely high accuracy and efficiency, with only subtle differences between each other. For 2B energies, they achieved $R^2 > 0.92$, |MSE| < 0.003 kcal/mol, and MAE < 0.28 kcal/mol for pure water, and $R^2 > 0.99$, |MSE| < 0.008 kcal/mol, and MAE < 0.15 kcal/mol for pure phenol and water–phenol mixture. Regarding 3B energies, they arrived at the best performance of $R^2 > 0.999$, |MSE| < 0.002 kcal/mol, and MAE < 0.013 kcal/mol for pure water, and $R^2 > 0.84$, |MSE| < 0.001 kcal/mol, and MAE < 0.06 kcal/mol for pure phenol and water–phenol mixture. The values of MSEs were universally negligible compared to the typical error bars of MP2 [90] and DFT [91], indicating the absence of systematic errors or biases in FBGNN-MBE. Similarly, all MAEs fell significantly below the threshold of chemical accuracy of 1 kcal/mol. Along with large values of R^2 they implied the potential of well-trained FBGNN models to replace MP2 or DFT in generating lower order terms in MBE with minimal deviations from the actual values. Additionally, the significant reductions in computational costs by more than 91.5% or higher confirmed that FBGNN-MBE can accelerate the

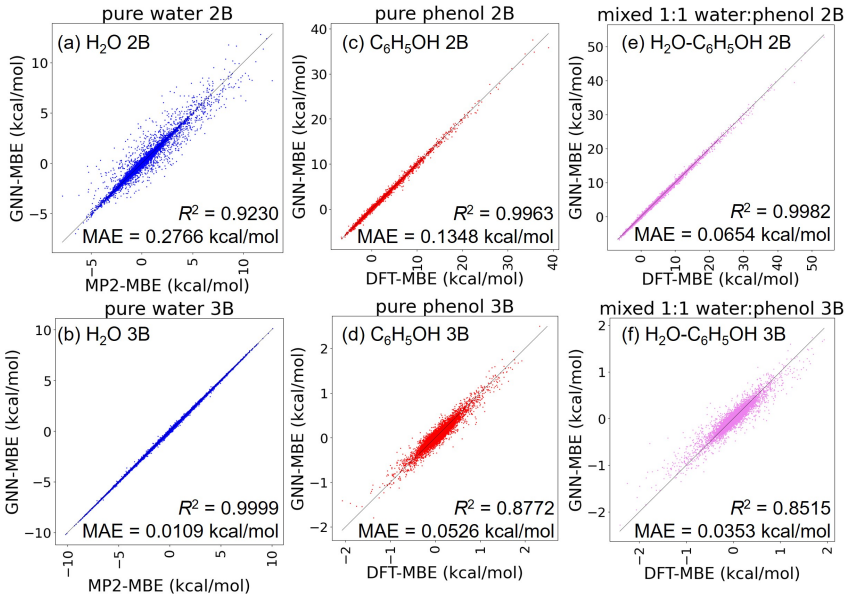

Figure 4: Comparison between PAMNet-predicted and MP2/DFT-evaluated 2B and 3B energies for all three benchmark systems.

fragment-based calculations by two to four orders of magnitude. This was because the computational complexity was decreased from N^5M^5 for MP2 and N^3M^5 for MP2-MBE to NM^5 for MP2-based FBGNN-MBE, or N^3M^3 for DFT and DFT-MBE to NM^3 for DFT-based FBGNN-MBE, for a system containing N fragments with M basis functions each fragment.

4.2 Comparison between MXMNet-MBE and PAMNet-MBE

We herein proved the marginally stronger performance of PAMNet-MBE compared to MXMNet-MBE due to the inclusion of the fusion module. Behaviors of MXMNet-MBE and PAMNet-MBE were similar, with PAMNet-MBE slightly outperforming MXMNet-MBE in accuracy and slightly underperforming in efficiency for 2B energies. For example, for pure phenol, MXMNet-MBE attained impressive $R^2 = 0.9955$ and MAE $= 0.1483$ kcal/mol and reduced the time cost by 99.92%, while PAMNet-MBE achieved $R^2 = 0.9963$ and MAE $= 0.1348$ kcal/mol and reduced the time cost by 99.88%. This result indicated that the implementation of the fusion module in PAMNet enhanced the capacity to capture moderate two-fragment interactions but introduced a minor increase in the computational cost. Regarding the larger and more sophisticated 3B energy data sets, PAMNet-MBE showed a higher efficiency in addition to a higher accuracy. From these observations we concluded that PAMNet was the preferred choice as a FBGNN for our current and future FBGNN-MBE tasks.

4.3 Comparison across Data Sets

We herein discussed the relationship between the natures and strengths of 2B and 3B interactions in a system and the behaviors of PAMNet-MBE and MXMNet-MBE. A comparison across different data sets reflected the character of these benchmark systems in addition to the accuracy of the FBGNN-MBE models. For example, all MAEs of 2B energies were significantly higher than 3B counterparts, because the magnitudes of 2B energies were usually greater than 3B energies. For a similar reason, due to the stronger hydrogen bonds in pure water (a few kcal/mol), its MAEs associated with 2B energies were also considerably higher than pure phenol and water–phenol mixture which were dominated by weaker van der Waals interactions. Moreover, for pure water both MXMNet-MBE and PAMNet-MBE exhibited a stronger performance in 3B energies than 2B energies, which was intriguing and counterintuitive but can be attributed to several factors. (a) Water trimers encompassed broader ranges of geometries and QM effects and a larger data set and offered more informative data for model training, while dimers were usually oversimplified by missing some critical interactions. (b) 3B terms from the $2\times$-density clusters incorporated both attractive (negative) and repulsive (positive)

effects, while the repulsion dominated in dimers, which were captured by the models. (c) Long-range interactions and polarizations prevailed in 3B interactions, which aligned with the model strength.

4.4 Comparison with Conventional GNN Models

We herein demonstrated the state-of-the-art accuracy of FBGNN-MBE. We conducted a comparative analysis against MBE approaches built upon several established GNN architectures at the frontier of computational chemistry and molecular representation learning, including SchNet [51], DimeNet [56] DimeNet++ [57], and ViSNet [60]. Using 2B and 3B energies of pure water clusters, we compared their accuracy in terms of the values of R^2 and MAEs (Table 3). For 2B energies, MXMNet-MBE and PAMNet-MBE achieved the highest R^2 values of 0.9400 and 0.9230, respectively, and the lowest MAEs of 0.2604 and 0.2766 kcal/mol, respectively. These results substantially outperformed any other model, which all showed $R^2 < 0.67$ (without obvious trends) and MAE > 0.86 kcal/mol (more than three times as much). The performance gap was equally pronounced for the 3B energies, where MXMNet-MBE and PAMNet-MBE achieved nearly-perfect R^2 values of 0.9998 and 0.9999, respectively, with remarkably low MAE values of 0.0121 and 0.0109 kcal/mol, respectively. While other models like DimeNet++-MBE also performed well on 3B energies ($R^2 = 0.9986$, MAE $= 0.0214$ kcal/mol), MXMNet-MBE and PAMNet-MBE still maintained a clear edge in accuracy. These results underlined the enhanced predictive accuracy of FBGNN-MBE models for both 2B and 3B interactions in water clusters characterized by moderate-strength hydrogen bonds, due to the the efficacy of FBGNNs in capturing the complexities of both attractive and repulsive interactions.

Table 3: Comparative Performance of FBGNN-MBE with Other GNN-MBE Models.

Data Set	H_2O 2B		H_2O 3B	
GNN Model	R^2	MAE (kcal/mol)	R^2	MAE (kcal/mol)
MXMNet	0.9400	0.2604	0.9998	0.0121
PAMNet	0.9230	0.2766	0.9999	0.0109
SchNet	0.6491	0.8756	0.9783	0.0957
DimeNet	0.6638	0.8796	0.9958	0.0240
DimeNet++	0.6545	0.8698	0.9986	0.0214
ViSNet	0.6532	0.8752		

4.5 Deeper Performance Analysis

We herein conducted a deeper analysis to understand the impact of the molecular density on the character of the electronic structures. We reported the average 2B and 3B energies from MP2 or DFT calculations as $\langle E_{\text{FP}} \rangle$ in Table 2. Across all benchmark systems, the values of $\langle E_{\text{FP}} \rangle$ for the 2B energies were always sizable positive values, while those for the 3B energies were either positive or negative but still negligible considering the error bars of MP2 and DFT. The behaviors of 2B energies were counterintuitive at first sight because we had expected attractive hydrogen bonds and van der Waals interactions, but can actually be attributed to the $2\times$ densities of these sampled clusters. We employed such $2\times$ densities because we wanted to ensure an inclusion of high energy configurations in the samples to treat the increased complexity, amplify the importance of hydrogen bonds, and promote the precise reproduction of 2B/3B interactions. However, this treatment also altered the physics of the interacting clusters. For example, by increasing the density and pressure, low-density water (LDW) transitions into high-density water (HDW) through the disruption of hydrogen bonds between the first and second coordination shells, resulting in significant structural shifts and more linear hydrogen bonding configurations [92]. At the same time, HDW illustrated a stronger (Pauli) repulsion between closely packed molecules to counteract the attractive hydrogen bonds. Both factors introduced sizable positive contributions for the 2B energies [93, 94]. The behaviors of 3B energies, though smaller in magnitude, were not significantly impacted by the high density and still reflected a complex interplay of cooperative and anti-cooperative effects [95, 96].

4.6 Sensitivity Analysis

We herein understood and optimized the model reliability of FBGNN-MBE in complex tasks like predicting 2B and 3B energies [97] to guide future design and improvement. We analyzed the sensitivity of FBGNN-MBE approaches over varying hyperparameters. We used R^2 coefficients and

MAEs of 2B and 3B energies as evaluation metrics. We presented detailed discussions about these hyperparameters in Section A.3, and summarized optimized values in Table 4.

Table 4: Summary of Optimized Hyperparameters

Model	Data set	N_{epoch}	N_{layer}	D_{gc} (Å)	D_{lc} (Å)	N_{batch}	k_{learn}
MXMNet	H_2O 2B	104	4	5.0	1.7	64	0.0001
	H_2O 3B	43	4	5.0	1.7	64	0.0001
	C_6H_5OH 2B	154	4	15.0	3.0	64	0.0001
	C_6H_5OH 3B	435	6	15.0	5.0	64	0.0001
	H_2O:C_6H_5OH 2B	494	4	10.0	5.0	64	0.0001
	H_2O:C_6H_5OH 3B	240	4	15.0	3.0	64	0.0001
PAMNet	H_2O 2B	207	2	5.0	1.7	64	0.0001
	H_2O 3B	66	6	5.0	1.7	64	0.0001
	C_6H_5OH 2B	256	4	15.0	3.0	64	0.0001
	C_6H_5OH 3B	54	3	15.0	5.0	64	0.0001
	H_2O:C_6H_5OH 2B	464	4	15.0	3.0	64	0.0001
	H_2O:C_6H_5OH 3B	78	4	15.0	4.0	64	0.0001

5 Conclusions and Future Directions

We presented FBGNN-MBE, a novel computational framework that hybridized FBGNNs with the MBE theory and exhibited enhanced robustness, accuracy, transferability, and interpretability from conventional NN- and GNN-accelerated QM models. Our method addressed the prohibitive computational costs of pure QM or QM-MBE methods in modeling aggregate and dynamic properties of large functional materials. In contrast to existing QM-MBE, we only evaluated 1B energies from first principles but generated nB ($n \geq 2$) energies based on structure–energy relationships trained by FBGNN. Instead of conventional GNN models, we implemented fragment-based MXMNet and PAMNet formalisms as backbone GNN approaches for a more intuitive alignment between model architecture and chemical hierarchy. Benchmarked on three clusters with different natures and strengths of intermolecular interactions, including pure water, pure phenol, and 1:1 water–phenol mixture, we revealed that well-trained FBGNN-MBE reached state-of-the-art chemical agreement with traditional QM-MBE models, with MAEs < 0.3 kcal/mol for 2B energies and < 0.02 kcal/mol for 3B energies, but reduced the computational cost by two to four orders of magnitude.

While our FBGNN-MBE framework was promising in both efficiency and accuracy, it exhibited at least two limitations that required our attentions in future developments. First, our training sets were created using $2\times$ molecular densities, which allowed us to sample high-energy configurations and enhance ergodicity and diversity of the data set, but also introduced biases towards repulsive 2B interactions [98]. Second, the present study focused on molecular aggregates with weak to moderate many-fragment interactions and the current fragmentation strategy did not cleave chemical bonds, so that the model transferability remained elusive. Finally, the present study did not implement the predictions for potential energy gradients (forces) or excited state energies. Looking ahead, we will apply FBGNN-MBE in the place of QM and QM-MBE in producing aggregate and dynamic properties that require on-the-fly evaluations of a FD-PES, such as Monte Carlo (MC) and MD simulations, and will extend the present framework beyond ground state electronic energies, such as optical band gaps and vibrational frequencies. We will enhance the model transferability to various chemical systems by implementing transfer learning [99]. We will improve the model capacity in physical interpretation by implementing the energy decomposition analysis (EDA) [100] so that we can quantitatively fraction the nB energies into different attractive and repulsive terms, such as electrostatics, Pauli repulsion, exchange–correlation, and dispersion. These applications will enhance the model potentials in the rational design of next-generation functional materials.

6 Acknowledgement

Z.L. and H.G. thank the financial support provided by UMass Amherst Start-Up Funds and NSF-UMass ADVANCE Collaborative Research Seed Grant. All authors thank the high-performance supercomputing resources provided by UMass/URI Unity Cluster and MIT Supercloud [101].

References

[1] Kaili Yao, Yujian Xia, Jun Li, Ning Wang, Jingrui Han, Congcong Gao, Mei Han, Guoqiang Shen, Yongchang Liu, Ali Seifitokaldani, Xuhui Sun, and Hongyan Liang. "Metal–organic framework derived copper catalysts for CO_2 to ethylene conversion". In: *Journal of Materials Chemistry A* 8 (22 2020), pp. 11117–11123. URL: http://doi.org/10.1039/D0TA02395G.

[2] Deqing Zhang, Cheng Li, Guanxin Zhang, Jianwu Tian, and Zitong Liu. "Phototunable and Photopatternable Polymer Semiconductors". In: *Accounts of Chemical Research* 57.4 (2024), pp. 625–635. URL: https://doi.org/10.1021/acs.accounts.3c00750.

[3] Yuhang Dong, Chi Yao, Yi Zhu, Lu Yang, Dan Luo, and Dayong Yang. "DNA Functional Materials Assembled from Branched DNA: Design, Synthesis, and Applications". In: *Chemical Reviews* 120.17 (2020), pp. 9420–9481. URL: https://doi.org/10.1021/acs.chemrev.0c00294.

[4] Chao Lu, Xiaohong Zhang, and Xi Chen. "Advanced Materials and Technologies toward Carbon Neutrality". In: *Accounts of Materials Research* 3.9 (2022), pp. 913–921. URL: https://doi.org/10.1021/accountsmr.2c00084.

[5] Chad A. Mirkin, Edward H. Sargent, and Daniel P. Schrag. "Energy transition needs new materials". In: *Science* 384.6697 (2024), pp. 713–713. URL: https://doi.org/10.1126/science.adq3799.

[6] Zhao Cheng, Rui Cao, Kangkang Wei, Yuhan Yao, Xinyu Liu, Jianlong Kang, Jianji Dong, Zhe Shi, Han Zhang, and Xinliang Zhang. "2D Materials Enabled Next-Generation Integrated Optoelectronics: from Fabrication to Applications". In: *Advanced Science* 8.11 (2021), p. 2003834. URL: https://doi.org/10.1002/advs.202003834.

[7] Chr. Møller and M. S. Plesset. "Note on an Approximation Treatment for Many-Electron Systems". In: *Physical Review* 46 (7 1934), pp. 618–622. URL: https://doi.org/10.1103/PhysRev.46.618.

[8] P. Hohenberg and W. Kohn. "Inhomogeneous Electron Gas". In: *Physical Review* 136 (3B 1964), B864–B871. URL: https://doi.org/10.1103/PhysRev.136.B864.

[9] W. Kohn and L. J. Sham. "Self-Consistent Equations Including Exchange and Correlation Effects". In: *Physical Review* 140 (4A 1965), A1133–A1138. URL: https://doi.org/10.1103/PhysRev.140.A1133.

[10] Trygve Helgaker, Poul Jørgensen, and Jeppe Olsen. "Perturbation Theory". In: *Molecular Electronic-Structure Theory*. John Wiley & Sons, Ltd, 2000. Chap. 14, pp. 724–816. URL: https://doi.org/10.1002/9781119019572.ch14.

[11] Stephan Mohr, Laura E. Ratcliff, Luigi Genovese, Damien Caliste, Paul Boulanger, Stefan Goedecker, and Thierry Deutsch. "Accurate and efficient linear scaling DFT calculations with universal applicability". In: *Physical Chemistry Chemical Physics* 17 (47 2015), pp. 31360–31370. URL: http://doi.org/10.1039/C5CP00437C.

[12] Qiming Sun and Garnet Kin-Lic Chan. "Quantum Embedding Theories". In: *Accounts of Chemical Research* 49.12 (2016), pp. 2705–2712. URL: https://doi.org/10.1021/acs.accounts.6b00356.

[13] John M. Herbert. "Fantasy versus reality in fragment-based quantum chemistry". In: *The Journal of Chemical Physics* 151.17 (2019), p. 170901. URL: https://doi.org/10.1063/1.5126216.

[14] Erin E. Dahlke and Donald G. Truhlar. "Electrostatically Embedded Many-Body Expansion for Simulations". In: *Journal of Chemical Theory and Computation* 4.1 (2008), pp. 1–6. URL: https://doi.org/10.1021/ct700223r.

[15] Ryan M. Richard, Ka Un Lao, and John M. Herbert. "Aiming for Benchmark Accuracy with the Many-Body Expansion". In: *Accounts of Chemical Research* 47.9 (2014), pp. 2828–2836. URL: https://doi.org/10.1021/ar500119q.

[16] Joseph P Heindel. "The Many-Body Expansion: A powerful tool for analyzing intermolecular interactions and driving molecular dynamics". PhD thesis. University of Washington, 2022. URL: http://hdl.handle.net/1773/48458.

[17] Ryan M. Richard and John M. Herbert. "A generalized many-body expansion and a unified view of fragment-based methods in electronic structure theory". In: *The Journal of Chemical Physics* 137.6 (2012), p. 064113. URL: https://doi.org/10.1063/1.4742816.

[18] Ryan M. Richard and John M. Herbert. "Many-Body Expansion with Overlapping Fragments: Analysis of Two Approaches". In: *Journal of Chemical Theory and Computation* 9.3 (2013), pp. 1408–1416. URL: https://doi.org/10.1021/ct300985h.

[19] Ryan M. Richard, Ka Un Lao, and John M. Herbert. "Achieving the CCSD(T) Basis-Set Limit in Sizable Molecular Clusters: Counterpoise Corrections for the Many-Body Expansion". In: *The Journal of Physical Chemistry Letters* 4.16 (2013), pp. 2674–2680. URL: https://doi.org/10.1021/jz401368u.

[20] Ryan M. Richard, Ka Un Lao, and John M. Herbert. "Understanding the many-body expansion for large systems. I. Precision considerations". In: *The Journal of Chemical Physics* 141.1 (2014), p. 014108. URL: https://doi.org/10.1063/1.4885846.

[21] Ka Un Lao, Kuan-Yu Liu, Ryan M. Richard, and John M. Herbert. "Understanding the many-body expansion for large systems. II. Accuracy considerations". In: *The Journal of Chemical Physics* 144.16 (2016), p. 164105. URL: https://doi.org/10.1063/1.4947087.

[22] Jie Liu and John M. Herbert. "Pair–Pair Approximation to the Generalized Many-Body Expansion: An Alternative to the Four-Body Expansion for ab Initio Prediction of Protein Energetics via Molecular Fragmentation". In: *Journal of Chemical Theory and Computation* 12.2 (2016), pp. 572–584. URL: https://doi.org/10.1021/acs.jctc.5b00955.

[23] Kuan-Yu Liu and John M. Herbert. "Understanding the many-body expansion for large systems. III. Critical role of four-body terms, counterpoise corrections, and cutoffs". In: *The Journal of Chemical Physics* 147.16 (2017), p. 161729. URL: https://doi.org/10.1063/1.4986110.

[24] Kuan-Yu Liu and John M. Herbert. "Energy-Screened Many-Body Expansion: A Practical Yet Accurate Fragmentation Method for Quantum Chemistry". In: *Journal of Chemical Theory and Computation* 16.1 (2020), pp. 475–487. URL: https://doi.org/10.1021/acs.jctc.9b01095.

[25] Dustin R. Broderick and John M. Herbert. "Scalable generalized screening for high-order terms in the many-body expansion: Algorithm, open-source implementation, and demonstration". In: *The Journal of Chemical Physics* 159.17 (2023), p. 174801. URL: https://doi.org/10.1063/5.0174293.

[26] Joseph P Heindel and Sotiris S. Xantheas. "The many-body expansion for aqueous systems revisited: I. Water–water interactions". In: *Journal of Chemical Theory and Computation* 16.11 (2020), pp. 6843–6855. URL: https://doi.org/10.1021/acs.jctc.9b00749.

[27] Joseph P. Heindel and Sotiris S. Xantheas. "The Many-Body Expansion for Aqueous Systems Revisited: II. Alkali Metal and Halide Ion–Water Interactions". In: *Journal of Chemical Theory and Computation* 17.4 (2021), pp. 2200–2216. URL: https://doi.org/10.1021/acs.jctc.0c01309.

[28] Joseph P. Heindel and Sotiris S. Xantheas. "Molecular Dynamics Driven by the Many-Body Expansion (MBE-MD)". In: *Journal of Chemical Theory and Computation* 17.12 (2021), pp. 7341–7352. URL: https://doi.org/10.1021/acs.jctc.1c00780.

[29] Joseph P. Heindel, Mikhail V. Kirov, and Sotiris S. Xantheas. "Hydrogen bond arrangements in $(H_2O)_{20,24,28}$ clathrate hydrate cages: Optimization and many-body analysis". In: *The Journal of Chemical Physics* 157.9 (2022), p. 094301. URL: https://doi.org/10.1063/5.0095335.

[30] Kristina M. Herman, Joseph P. Heindel, and Sotiris S. Xantheas. "The many-body expansion for aqueous systems revisited: III. Hofmeister ion–water interactions". In: *Physical Chemistry Chemical Physics* 23 (19 2021), pp. 11196–11210. URL: http://doi.org/10.1039/D1CP00409C.

[31] Kristina M. Herman, Anthony J. Stone, and Sotiris S. Xantheas. "A classical model for three-body interactions in aqueous ionic systems". In: *The Journal of Chemical Physics* 157.2 (2022), p. 024101. URL: https://doi.org/10.1063/5.0095739.

[32] Kristina M. Herman, Anthony J. Stone, and Sotiris S. Xantheas. "Accurate Calculation of Many-Body Energies in Water Clusters Using a Classical Geometry-Dependent Induction Model". In: *Journal of Chemical Theory and Computation* 19.19 (2023), pp. 6805–6815. URL: https://doi.org/10.1021/acs.jctc.3c00575.

[33] Kristina M. Herman and Sotiris S. Xantheas. "An extensive assessment of the performance of pairwise and many-body interaction potentials in reproducing ab initio benchmark binding energies for water clusters $n = 2 - 25$". In: *Physical Chemistry Chemical Physics* 25 (10 2023), pp. 7120–7143. URL: http://doi.org/10.1039/D2CP03241D.

[34] Kristina M. Herman and Sotiris S. Xantheas. "A Formulation of the Many-Body Expansion (MBE) for Periodic Systems: Application to Several Ice Phases". In: *The Journal of Physical Chemistry Letters* 14.4 (2023), pp. 989–999. URL: https://doi.org/10.1021/acs.jpclett.2c03822.

[35] Joani Mato, Demeter Tzeli, and Sotiris S. Xantheas. "The many-body expansion for metals. I. The alkaline earth metals Be, Mg, and Ca". In: *The Journal of Chemical Physics* 157.8 (2022), p. 084313. URL: https://doi.org/10.1063/5.0094598.

[36] Theodore Depastas, George A. Souliotis, Demeter Tzeli, and Sotiris S. Xantheas. "Many-body expansion for light nuclear systems". In: *Physical Review C* 107 (4 2023), p. 044004. URL: https://doi.org/10.1103/PhysRevC.107.044004.

[37] Kristof T Schütt, Farhad Arbabzadah, Stefan Chmiela, Klaus R Müller, and Alexandre Tkatchenko. "Quantum-Chemical Insights From Deep Tensor Neural Networks". In: *Nature Communications* 8.1 (2017), p. 13890. URL: https://doi.org/10.1038/ncomms13890.

[38] John A Keith, Valentin Vassilev-Galindo, Bingqing Cheng, Stefan Chmiela, Michael Gastegger, Klaus-Robert Müller, and Alexandre Tkatchenko. "Combining Machine Learning and Computational Chemistry for Predictive Insights Into Chemical Systems". In: *Chemical Reviews* 121.16 (2021), pp. 9816–9872. URL: https://doi.org/10.1021/acs.chemrev.1c00107.

[39] Yaolong Zhang, Qidong Lin, and Bin Jiang. "Atomistic neural network representations for chemical dynamics simulations of molecular, condensed phase, and interfacial systems: Efficiency, representability, and generalization". In: *WIREs Computational Molecular Science* 13.3 (2023), e1645. URL: https://doi.org/10.1002/wcms.1645.

[40] Kun Yao, John E Herr, and John Parkhill. "The Many-Body Expansion Combined With Neural Networks". In: *The Journal of Chemical Physics* 146.1 (2017), p. 014106. URL: https://doi.org/10.1063/1.4973380.

[41] Stefan Chmiela, Alexandre Tkatchenko, Huziel E. Sauceda, Igor Poltavsky, Kristof T. Schütt, and Klaus-Robert Müller. "Machine learning of accurate energy-conserving molecular force fields". In: *Science Advances* 3.5 (2017), e1603015. URL: https://doi.org/10.1126/sciadv.1603015.

[42] Justin Gilmer, Samuel S. Schoenholz, Patrick F. Riley, Oriol Vinyals, and George E. Dahl. "Neural Message Passing for Quantum Chemistry". In: *Proceedings of the 34th International Conference on Machine Learning*. Ed. by Doina Precup and Yee Whye Teh. Vol. 70. Proceedings of Machine Learning Research. PMLR, 2017, pp. 1263–1272. URL: https://proceedings.mlr.press/v70/gilmer17a.html.

[43] Kun Yao, John E. Herr, David W. Toth, Ryker Mckintyre, and John Parkhill. "The TensorMol-0.1 model chemistry: A neural network augmented with long-range physics". In: *Chemical Science* 9 (8 2018), pp. 2261–2269. URL: http://doi.org/10.1039/C7SC04934J.

[44] Thomas N. Kipf and Max Welling. "Semi-Supervised Classification with Graph Convolutional Networks". In: *International Conference on Learning Representations*. 2017. URL: https://openreview.net/forum?id=SJU4ayYgl.

[45] Will Hamilton, Zhitao Ying, and Jure Leskovec. "Inductive Representation Learning on Large Graphs". In: *Advances in Neural Information Processing Systems*. Ed. by I. Guyon, U. Von Luxburg, S. Bengio, H. Wallach, R. Fergus, S. Vishwanathan, and R. Garnett. Vol. 30. Curran Associates, Inc., 2017. URL: https://proceedings.neurips.cc/paper_files/paper/2017/file/5dd9db5e033da9c6fb5ba83c7a7ebea9-Paper.pdf.

[46] Jörg Behler and Michele Parrinello. "Generalized neural-network representation of high-dimensional potential-energy surfaces". In: *Physical Review Letters* 98.14 (2007), p. 146401. URL: https://doi.org/10.1103/PhysRevLett.98.146401.

[47] Giuseppe Carleo and Matthias Troyer. "Solving the quantum many-body problem with artificial neural networks". In: *Science* 355.6325 (2017), pp. 602–606. URL: https://doi.org/science.aag2302.

[48] Chi Chen, Weike Ye, Yunxing Zuo, Chen Zheng, and Shyue Ping Ong. "Graph networks as a universal machine learning framework for molecules and crystals". In: *Chemistry of Materials* 31.9 (2019), pp. 3564–3572. URL: https://doi.org/10.1021/acs.chemmater.9b01294.

[49] Minyi Dai, Mehmet F Demirel, Yingyu Liang, and Jia-Mian Hu. "Graph neural networks for an accurate and interpretable prediction of the properties of polycrystalline materials". In: *npj Computational Materials* 7 (2021), p. 103. URL: https://doi.org/10.1038/s41524-021-00574-w.

[50] Minyi Dai, Mehmet F Demirel, Yingyu Liang, and Jia-Mian Hu. "Author Correction: Graph neural networks for an accurate and interpretable prediction of the properties of polycrystalline materials". In: *npj Computational Materials* 8 (2022), p. 122. URL: https://doi.org/10.1038/s41524-022-00804-9.

[51] Kristof T. Schütt, Huziel E. Sauceda, Pieter-Jan Kindermans, Alexandre Tkatchenko, and Klaus-Robert Müller. "SchNet – A Deep Learning Architecture for Molecules and Materials". In: *The Journal of Chemical Physics* 148.24 (2018), p. 241722. URL: https://doi.org/10.1063/1.5019779.

[52] Octavian Ganea, Lagnajit Pattanaik, Connor Coley, Regina Barzilay, Klavs Jensen, William Green, and Tommi Jaakkola. "GeoMol: Torsional Geometric Generation of Molecular 3D Conformer Ensembles". In: *Advances in Neural Information Processing Systems*. Ed. by M. Ranzato, A. Beygelzimer, Y. Dauphin, P.S. Liang, and J. Wortman Vaughan. Vol. 34. Curran Associates, Inc., 2021, pp. 13757–13769. URL: https://proceedings.neurips.cc/paper_files/paper/2021/file/725215ed82ab6306919b485b81ff9615-Paper.pdf.

[53] Hanxuan Cai, Huimin Zhang, Duancheng Zhao, Jingxing Wu, and Ling Wang. "FP-GNN: a versatile deep learning architecture for enhanced molecular property prediction". In: *Briefings in Bioinformatics* 23.6 (2022), bbac408. URL: https://doi.org/10.1093/bib/bbac408.

[54] Xiangzhe Kong, Wenbing Huang, and Yang Liu. "End-to-End Full-Atom Antibody Design". In: *Proceedings of the 40th International Conference on Machine Learning*. Ed. by Andreas Krause, Emma Brunskill, Kyunghyun Cho, Barbara Engelhardt, Sivan Sabato, and Jonathan Scarlett. Vol. 202. Proceedings of Machine Learning Research. PMLR, 2023, pp. 17409–17429. URL: https://proceedings.mlr.press/v202/kong23c.html.

[55] Oliver T Unke and Markus Meuwly. "PhysNet: A neural network for predicting energies, forces, dipole moments, and partial charges". In: *Journal of Chemical Theory and Computation* 15.6 (2019), pp. 3678–3693. URL: http://doi.org/10.1021/acs.jctc.9b00181.

[56] Johannes Gasteiger, Janek Groß, and Stephan Günnemann. "Directional Message Passing for Molecular Graphs". In: *International Conference on Learning Representations*. 2020. URL: https://openreview.net/forum?id=B1eWbxStPH.

[57] Johannes Gasteiger, Shankari Giri, Johannes T Margraf, and Stephan Günnemann. "Fast and uncertainty-aware directional message passing for non-equilibrium molecules". In: *arXiv* (2020), p. 2011.14115. URL: https://doi.org/10.48550/arXiv.2004.11198.

[58] Víctor Garcia Satorras, Emiel Hoogeboom, and Max Welling. "E(n) Equivariant Graph Neural Networks". In: *Proceedings of the 38th International Conference on Machine Learning*. Ed. by Marina Meila and Tong Zhang. Vol. 139. Proceedings of Machine Learning Research. PMLR, 2021, pp. 9323–9332. URL: https://proceedings.mlr.press/v139/satorras21a.html.

[59] Johannes Brandstetter, Rob Hesselink, Elise van der Pol, Erik J. Bekkers, and Max Welling. "Geometric and Physical Quantities improve E(3) Equivariant Message Passing". In: *International Conference on Learning Representations*. 2022. URL: https://openreview.net/forum?id=_xwr8gOBeV1.

[60] Yusong Wang, Tong Wang, Shaoning Li, Xinheng He, Mingyu Li, Zun Wang, Nanning Zheng, Bin Shao, and Tie-Yan Liu. "Enhancing geometric representations for molecules with equivariant vector-scalar interactive message passing". In: *Nature Communications* 15.1 (2024), p. 313. URL: https://doi.org/10.1038/s41467-023-43720-2.

[61] Thijs Stuyver and Connor W. Coley. "Quantum chemistry-augmented neural networks for reactivity prediction: Performance, generalizability, and explainability". In: *The Journal of Chemical Physics* 156.8 (2022), p. 084104. URL: https://doi.org/10.1063/5.0079574.

[62] Saian Chen, Aziguli Wulamu, Qiping Zou, Han Zheng, Li Wen, Xi Guo, Han Chen, Taohong Zhang, and Ying Zhang. "MD-GNN: A mechanism-data-driven graph neural network for molecular properties prediction and new material discovery". In: *Journal of Molecular Graphics and Modelling* 123 (2023), p. 108506. URL: https://doi.org/10.1016/j.jmgm.2023.108506.

[63] Xiao-Shuang Li, Xiang Liu, Le Lu, Xian-Sheng Hua, Ying Chi, and Kelin Xia. "Multiphysical graph neural network (MP-GNN) for COVID-19 drug design". In: *Briefings in Bioinformatics* 23.4 (2022), bbac231. URL: https://doi.org/10.1093/bib/bbac231.

[64] Shuke Zhang, Yanzhao Jin, Tianmeng Liu, Qi Wang, Zhaohui Zhang, Shuliang Zhao, and Bo Shan. "SS-GNN: a simple-structured graph neural network for affinity prediction". In: *ACS Omega* 8.25 (2023), pp. 22496–22507. URL: https://doi.org/10.1021/acsomega.3c00085.

[65] Emily Alsentzer, Samuel Finlayson, Michelle Li, and Marinka Zitnik. "Subgraph Neural Networks". In: *Advances in Neural Information Processing Systems*. Ed. by H. Larochelle, M. Ranzato, R. Hadsell, M.F. Balcan, and H. Lin. Vol. 33. Curran Associates, Inc., 2020, pp. 8017–8029. URL: https://proceedings.neurips.cc/paper_files/paper/2020/file/5bca8566db79f3788be9efd96c9ed70d-Paper.pdf.

[66] Eric M. Collins and Krishnan Raghavachari. "A Fragmentation-Based Graph Embedding Framework for QM/ML". In: *The Journal of Physical Chemistry A* 125.31 (2021), pp. 6872–6880. URL: https://doi.org/10.1021/acs.jpca.1c06152.

[67] Xiaoyu Chen and Quan Qian. "subGE: Enhancing the subgraph representation of molecular compounds structure–activity relationship discovery". In: *Engineering Applications of Artificial Intelligence* 119 (2023), p. 105727. URL: https://doi.org/10.1016/j.engappai.2022.105727.

[68] Shuo Zhang, Yang Liu, and Lei Xie. "Molecular Mechanics-Driven Graph Neural Network With Multiplex Graph for Molecular Structures". In: *arXiv* (2020), p. 2011.07457. URL: https://doi.org/10.48550/arXiv.2011.07457.

[69] Shuo Zhang, Yang Liu, and Lei Xie. "A universal framework for accurate and efficient geometric deep learning of molecular systems". In: *Scientific Reports* 13.1 (2023), p. 19171. URL: https://doi.org/10.1038/s41598-023-46382-8.

[70] Raghunathan Ramakrishnan, Pavlo O. Dral, Matthias Rupp, and O. Anatole Von Lilienfeld. "Quantum Chemistry Structures and Properties of 134 Kilo Molecules". In: *Scientific Data volume* 1 (2014), p. 140022. URL: https://doi.org/10.1038/sdata.2014.22.

[71] Renxiao Wang, Xueliang Fang, Yipin Lu, Chao-Yie Yang, and Shaomeng Wang. "The PDBbind Database: Methodologies and Updates". In: *Journal of Medicinal Chemistry* 48.12 (2005), pp. 4111–4119. URL: https://doi.org/10.1021/jm048957q.

[72] Raphael J. L. Townshend, Stephan Eismann, Andrew M. Watkins, Ramya Rangan, Masha Karelina, Rhiju Das, and Ron O. Dror. "Geometric deep learning of RNA structure". In: *Science* 373.6558 (2021), pp. 1047–1051. URL: https://doi.org/10.1126/science.abe5650.

[73] William L Hamilton. "Graph Representation Learning". In: *Synthesis Lectures on Artifical Intelligence and Machine Learning* 14.3 (2020), pp. 1–159. URL: https://doi.org/10.1007/978-3-031-01588-5.

[74] Matthias Rupp, Alexandre Tkatchenko, Klaus-Robert Müller, and O. Anatole von Lilienfeld. "Fast and Accurate Modeling of Molecular Atomization Energies with Machine Learning". In: *Physical Review Letters* 108 (5 2012), p. 058301. URL: https://doi.org/10.1103/PhysRevLett.108.058301.

[75] Xunqiang Jiang, Yuanfu Lu, Yuan Fang, and Chuan Shi. "Contrastive Pre-Training of GNNs on Heterogeneous Graphs". In: *Proceedings of the 30th ACM International Conference on Information & Knowledge Management*. CIKM '21. Association for Computing Machinery, 2021, pp. 803–812. URL: https://doi.org/10.1145/3459637.3482332.

[76] Xiao Wang, Deyu Bo, Chuan Shi, Shaohua Fan, Yanfang Ye, and S Yu Philip. "A survey on heterogeneous graph embedding: methods, techniques, applications and sources". In: *IEEE Transactions on Big Data* 9.2 (2023), pp. 415–436. URL: https://doi.org/10.1109/TBDATA.2022.3177455.

[77] Diederik P Kingma and Jimmy Ba. "Adam: A method for stochastic optimization". In: *arXiv* (2017), p. 1412.6980. URL: https://doi.org/10.48550/arXiv.1412.6980.

[78] Gennady Yu Gor, Salla Tapio, Alexandra V Domanskaya, Markku Räsänen, Alexander V Nemukhin, and Leonid Khriachtchev. "Matrix-isolation study of the phenol–water complex and phenol dimer". In: *Chemical Physics Letters* 517.1-3 (2011), pp. 9–15. URL: https://doi.org/10.1016/j.cplett.2011.09.089.

[79] Ning Zhang, Xuehua Ruan, Yuechun Song, Zhao Liu, and Gaohong He. "Molecular dynamics simulation of the hydration structure and hydrogen bonding behavior of phenol in aqueous solution". In: *Journal of Molecular Liquids* 221 (2016), pp. 942–948. URL: https://doi.org/10.1016/j.molliq.2016.06.048.

[80] Mark James Abraham, Teemu Murtola, Roland Schulz, Szilárd Páll, Jeremy C Smith, Berk Hess, and Erik Lindahl. "GROMACS: High performance molecular simulations through multi-level parallelism from laptops to supercomputers". In: *SoftwareX* 1 (2015), pp. 19–25. URL: https://doi.org/10.1016/j.softx.2015.06.001.

[81] Leandro Martínez, Ricardo Andrade, Ernesto G Birgin, and José Mario Martínez. "PACKMOL: A package for building initial configurations for molecular dynamics simulations". In: *Journal of Computational Chemistry* 30.13 (2009), pp. 2157–2164. URL: https://doi.org/10.1002/jcc.21224.

[82] Martin P. Head-Gordon, John A. Pople, and Michael J. Frisch. "MP2 energy evaluation by direct methods". In: *Chemical Physics Letters* 153.6 (1988), pp. 503–506. URL: https://doi.org/10.1016/0009-2614(88)85250-3.

[83] Jr. Dunning Thom H. "Gaussian basis sets for use in correlated molecular calculations. I. The atoms boron through neon and hydrogen". In: *The Journal of Chemical Physics* 90.2 (1989), pp. 1007–1023. URL: https://doi.org/10.1063/1.456153.

[84] Rick A. Kendall, Thom H. Dunning Jr., and Robert J. Harrison. "Electron affinities of the first-row atoms revisited. Systematic basis sets and wave functions". In: *The Journal of Chemical Physics* 96.9 (1992), pp. 6796–6806. URL: https://doi.org/10.1063/1.462569.

[85] You-Sheng Lin, Guan-De Li, Shan-Ping Mao, and Jeng-Da Chai. "Long-range corrected hybrid density functionals with improved dispersion corrections". In: *Journal of Chemical Theory and Computation* 9.1 (2013), pp. 263–272. URL: https://doi.org/10.1021/ct300715s.

[86] R. Krishnan, J. S. Binkley, R. Seeger, and J. A. Pople. "Self-consistent molecular orbital methods. XX. A basis set for correlated wave functions". In: *The Journal of Chemical Physics* 72.1 (1980), pp. 650–654. URL: https://doi.org/10.1063/1.438955.

[87] Evgeny Epifanovsky, Andrew T. B. Gilbert, Xintian Feng, Joonho Lee, Yuezhi Mao, Narbe Mardirossian, Pavel Pokhilko, Alec F. White, Marc P. Coons, Adrian L. Dempwolff, Zhengting Gan, Diptarka Hait, Paul R. Horn, Leif D. Jacobson, Ilya Kaliman, Jörg Kussmann, Adrian W. Lange, Ka Un Lao, Daniel S. Levine, Jie Liu, Simon C. McKenzie, Adrian F. Morrison, Kaushik D. Nanda, Felix Plasser, Dirk R. Rehn, Marta L. Vidal, Zhi-Qiang You, Ying Zhu, Bushra Alam, Benjamin J. Albrecht, Abdulrahman Aldossary, Ethan Alguire, Josefine H. Andersen, Vishikh Athavale, Dennis Barton, Khadiza Begam, Andrew Behn, Nicole Bellonzi, Yves A. Bernard, Eric J. Berquist, Hugh G. A. Burton, Abel Carreras, Kevin Carter-Fenk, Romit Chakraborty, Alan D. Chien, Kristina D. Closser, Vale Cofer-Shabica, Saswata Dasgupta, Marc de Wergifosse, Jia Deng, Michael Diedenhofen, Hainam Do, Sebastian Ehlert, Po-Tung Fang, Shervin Fatehi, Qingguo Feng, Triet Friedhoff, James Gayvert, Qinghui Ge, Gergely Gidofalvi, Matthew Goldey, Joe Gomes, Cristina E. González-Espinoza, Sahil Gulania, Anastasia O. Gunina, Magnus W. D. Hanson-Heine, Phillip H. P. Harbach, Andreas Hauser, Michael F. Herbst, Mario Hernández Vera, Manuel Hodecker, Zachary C. Holden, Shannon Houck, Xunkun Huang, Kerwin Hui, Bang C. Huynh, Maxim Ivanov, ádám Jász, Hyunjun Ji, Hanjie Jiang, Benjamin Kaduk, Sven Kähler, Kirill Khistyaev, Jaehoon Kim, Gergely Kis, Phil Klunzinger, Zsuzsanna Koczor-Benda, Joong Hoon Koh, Dimitri Kosenkov, Laura Koulias, Tim Kowalczyk, Caroline M. Krauter, Karl Kue, Alexander Kunitsa, Thomas Kus, István Ladjánszki, Arie Landau, Keith V. Lawler, Daniel Lefrancois, Susi Lehtola, Run R. Li, Yi-Pei Li, Jiashu Liang, Marcus Liebenthal, Hung-Hsuan Lin, You-Sheng Lin, Fenglai Liu, Kuan-Yu Liu, Matthias Loipersberger, Arne Luenser, Aaditya Manjanath, Prashant Manohar, Erum Mansoor, Sam F. Manzer, Shan-Ping Mao, Aleksandr V. Marenich, Thomas Markovich, Stephen Mason, Simon A. Maurer, Peter F. McLaughlin, Maximilian F. S. J. Menger, Jan-Michael Mewes, Stefanie A. Mewes, Pierpaolo Morgante, J. Wayne Mullinax, Katherine J. Oosterbaan, Garrette Paran, Alexander C. Paul, Suranjan K. Paul, Fabijan Pavošević, Zheng Pei, Stefan Prager, Emil I. Proynov, ádám Rák, Eloy

Ramos-Cordoba, Bhaskar Rana, Alan E. Rask, Adam Rettig, Ryan M. Richard, Fazle Rob, Elliot Rossomme, Tarek Scheele, Maximilian Scheurer, Matthias Schneider, Nickolai Sergueev, Shaama M. Sharada, Wojciech Skomorowski, David W. Small, Christopher J. Stein, Yu-Chuan Su, Eric J. Sundstrom, Zhen Tao, Jonathan Thirman, Gábor J. Tornai, Takashi Tsuchimochi, Norm M. Tubman, Srimukh Prasad Veccham, Oleg Vydrov, Jan Wenzel, Jon Witte, Atsushi Yamada, Kun Yao, Sina Yeganeh, Shane R. Yost, Alexander Zech, Igor Ying Zhang, Xing Zhang, Yu Zhang, Dmitry Zuev, Alán Aspuru-Guzik, Alexis T. Bell, Nicholas A. Besley, Ksenia B. Bravaya, Bernard R. Brooks, David Casanova, Jeng-Da Chai, Sonia Coriani, Christopher J. Cramer, György Cserey, A. Eugene DePrince, Robert A. DiStasio, Andreas Dreuw, Barry D. Dunietz, Thomas R. Furlani, William A. Goddard, Sharon Hammes-Schiffer, Teresa Head-Gordon, Warren J. Hehre, Chao-Ping Hsu, Thomas-C. Jagau, Yousung Jung, Andreas Klamt, Jing Kong, Daniel S. Lambrecht, WanZhen Liang, Nicholas J. Mayhall, C. William McCurdy, Jeffrey B. Neaton, Christian Ochsenfeld, John A. Parkhill, Roberto Peverati, Vitaly A. Rassolov, Yihan Shao, Lyudmila V. Slipchenko, Tim Stauch, Ryan P. Steele, Joseph E. Subotnik, Alex J. W. Thom, Alexandre Tkatchenko, Donald G. Truhlar, Troy Van Voorhis, Tomasz A. Wesolowski, K. Birgitta Whaley, H. Lee Woodcock, Paul M. Zimmerman, Shirin Faraji, Peter M. W. Gill, Martin Head-Gordon, John M. Herbert, and Anna I. Krylov. "Software for the Frontiers of Quantum Chemistry: An Overview of Developments in the Q-Chem 5 Package". In: *The Journal of Chemical Physics* 155 (8 2021), p. 084801. URL: http://doi.org/10.1063/5.0055522.

[88] James Bergstra, Rémi Bardenet, Yoshua Bengio, and Balázs Kégl. "Algorithms for Hyper-Parameter Optimization". In: *Advances in Neural Information Processing Systems*. Ed. by J. Shawe-Taylor, R. Zemel, P. Bartlett, F. Pereira, and K.Q. Weinberger. Vol. 24. Curran Associates, Inc., 2011. URL: https://proceedings.neurips.cc/paper_files/paper/2011/file/86e8f7ab32cfd12577bc2619bc635690-Paper.pdf.

[89] Dejun Jiang, Zhenxing Wu, Chang-Yu Hsieh, Guangyong Chen, Ben Liao, Zhe Wang, Chao Shen, Dongsheng Cao, Jian Wu, and Tingjun Hou. "Could graph neural networks learn better molecular representation for drug discovery? A comparison study of descriptor-based and graph-based models". In: *Journal of Cheminformatics* 13.1 (2021), pp. 1–23. URL: https://doi.org/10.1186/s13321-020-00479-8.

[90] Kevin E. Riley, James A. Platts, Jan Řezáč, Pavel Hobza, and J. Grant Hill. "Assessment of the Performance of MP2 and MP2 Variants for the Treatment of Noncovalent Interactions". In: *The Journal of Physical Chemistry A* 116.16 (2012), pp. 4159–4169. DOI: 10.1021/jp211997b. URL: https://doi.org/10.1021/jp211997b.

[91] Simuck F. Yuk, Irmak Sargin, Noah Meyer, Jaron T. Krogel, Scott P. Beckman, and Valentino R. Cooper. "Putting error bars on density functional theory". In: *Scientific Reports* 14.1 (2024), p. 20219. URL: https://doi.org/10.1038/s41598-024-69194-w.

[92] Alan K Soper and Maria Antonietta Ricci. "Structures of high-density and low-density water". In: *Physical Review Letters* 84.13 (2000), pp. 2881–2884. URL: https://doi.org/10.1103/PhysRevLett.84.2881.

[93] Anthony J Stone. *The theory of intermolecular forces*. 2nd. 2013. URL: https://doi.org/10.1093/acprof:oso/9780199672394.001.0001.

[94] Andreas Heßelmann. "Improved supermolecular second order Møller–Plesset intermolecular interaction energies using time-dependent density functional response theory". In: *The Journal of Chemical Physics* 128.14 (2008), p. 144112. URL: https://doi.org/10.1063/1.2905808.

[95] A Subha Mahadevi and G Narahari Sastry. "Cooperativity in noncovalent interactions". In: *Chemical Reviews* 116.5 (2016), pp. 2775–2825. URL: https://doi.org/10.1021/cr500344e.

[96] Sławomir Janusz Grabowski. "What is the covalency of hydrogen bonding?" In: *Chemical Reviews* 111.4 (2011), pp. 2597–2625. URL: https://doi.org/10.1021/cr800346f.

[97] Chirag Agarwal, Owen Queen, Himabindu Lakkaraju, and Marinka Zitnik. "Evaluating explainability for graph neural networks". In: *Scientific Data* 10.1 (2023), p. 144. URL: https://doi.org/10.1038/s41597-023-01974-x.

[98] Oliver T. Unke, Stefan Chmiela, Huziel E. Sauceda, Michael Gastegger, Igor Poltavsky, Kristof T. Schütt, Alexandre Tkatchenko, and Klaus-Robert Müller. "Machine Learning

Force Fields". In: *Chemical Reviews* 121.16 (2021), pp. 10142–10186. URL: https://doi.org/10.1021/acs.chemrev.0c01111.

[99] David Buterez, Jon Paul Janet, Steven J Kiddle, Dino Oglic, and Pietro Lió. "Transfer learning with graph neural networks for improved molecular property prediction in the multi-fidelity setting". In: *Nature Communications* 15.1 (2024), p. 1517. URL: https://doi.org/10.1038/s41467-024-45566-8.

[100] Lili Zhao, Moritz von Hopffgarten, Diego M. Andrada, and Gernot Frenking. "Energy decomposition analysis". In: *WIREs Computational Molecular Science* 8.3 (2018), e1345. URL: https://doi.org/10.1002/wcms.1345.

[101] Albert Reuther, Jeremy Kepner, Chansup Byun, Siddharth Samsi, William Arcand, David Bestor, Bill Bergeron, Vijay Gadepally, Michael Houle, Matthew Hubbell, Michael Jones, Anna Klein, Lauren Milechin, Julia Mullen, Andrew Prout, Antonio Rosa, Charles Yee, and Peter Michaleas. "Interactive Supercomputing on 40,000 Cores for Machine Learning and Data Analysis". In: *2018 IEEE High Performance extreme Computing Conference (HPEC)*. 2018, pp. 1–6. URL: https://doi.org/10.1109/HPEC.2018.8547629.

[102] F. Zahariev and M. S. Gordon. "Combined quantum Monte Carlo – effective fragment molecular orbital method: fragmentation across covalent bonds". In: *Physical Chemistry Chemical Physics* 23 (26 2021), pp. 14308–14314. URL: http://doi.org/10.1039/D0CP06528E.

[103] Xiang Song, Runjie Ma, Jiahang Li, Muhan Zhang, and David Paul Wipf. "Network in graph neural network". In: *arXiv* (2021), p. 2111.11638. URL: https://doi.org/10.48550/arXiv.2111.11638.

[104] Xiao-Meng Zhang, Li Liang, Lin Liu, and Ming-Jing Tang. "Graph Neural Networks and Their Current Applications in Bioinformatics". In: *Frontiers in Genetics* 12 (2021). URL: https://doi.org/10.3389/fgene.2021.690049.

[105] I. D. Brown. "On the geometry of O−H$\cdots$O hydrogen bonds". In: *Acta Crystallographica Section A: Crystal Physics, Diffraction, Theoretical and General Crystallography* 32.1 (1976), pp. 24–31. URL: https://doi.org/10.1107/S0567739476000041.

[106] J. N. Scott and J. M. Vanderkooi. "A new hydrogen bond angle/distance potential energy surface of the quantum water dimer". In: *Water* 2 (2010), pp. 14–28. URL: http://doi.org/10.14294/WATER.2010.1.

[107] Daniel Herschlag and Margaux M. Pinney. "Hydrogen Bonds: Simple after All?" In: *Biochemistry* 57.24 (2018), pp. 3338–3352. URL: https://doi.org/10.1021/acs.biochem.8b00217.

[108] Xin Liu, Yuxiang Zhang, Meng Wu, Mingyu Yan, Kun He, Wei Yan, Shirui Pan, Xiaochun Ye, and Dongrui Fan. "Revisiting Edge Perturbation for Graph Neural Network in Graph Data Augmentation and Attack". In: *arXiv* (2024), p. 2403.07943. URL: https://arxiv.org/abs/2403.07943.

[109] Anjan Chowdhury, Sriram Srinivasan, Animesh Mukherjee, Sanjukta Bhowmick, and Kuntal Ghosh. "Improving Node Classification Accuracy of GNN through Input and Output Intervention". In: *ACM Transactions on Knowledge Discovery from Data* 18.1 (2023). URL: https://doi.org/10.1145/3610535.

[110] Alessandro Rognoni, Riccardo Conte, and Michele Ceotto. "How many water molecules are needed to solvate one?" In: *Chemical Science* 12 (6 2021), pp. 2060–2064. URL: http://doi.org/10.1039/D0SC05785A.

[111] Hongfei Wu, Lijun Wu, Guoqing Liu, Zhirong Liu, Bin Shao, and Zun Wang. "SE3Set: Harnessing equivariant hypergraph neural networks for molecular representation learning". In: *arXiv preprint arXiv:2405.16511* (2024). URL: https://doi.org/10.48550/arXiv.2405.16511.

[112] Ilyes Batatia, Dávid Péter Kovács, Gregor N. C. Simm, Christoph Ortner, and Gábor Csányi. "MACE: Higher Order Equivariant Message Passing Neural Networks for Fast and Accurate Force Fields". In: *Advances in Neural Information Processing Systems*. Ed. by S. Koyejo, S. Mohamed, A. Agarwal, D. Belgrave, K. Cho, and A. Oh. Vol. 35. Curran Associates, Inc., 2022, pp. 11423–11436. URL: https://proceedings.neurips.cc/paper_files/paper/2022/file/4a36c3c51af11ed9f34615b81edb5bbc-Paper-Conference.pdf.

[113] Zaixi Zhang, Qi Liu, Hao Wang, Chengqiang Lu, and Chee-Kong Lee. "Motif-based Graph Self-Supervised Learning for Molecular Property Prediction". In: *Advances in Neural Information Processing Systems*. Ed. by M. Ranzato, A. Beygelzimer, Y. Dauphin, P.S. Liang, and J. Wortman Vaughan. Vol. 34. Curran Associates, Inc., 2021, pp. 15870–15882. URL: https://papers.neurips.cc/paper_files/paper/2021/file/85267d349a5e647ff0a9edcb5ffd1e02-Paper.pdf.

[114] Mesfin Diro Chaka, Chernet Amente Geffe, Alex Rodriguez, Nicola Seriani, Qin Wu, and Yedilfana Setarge Mekonnen. "High-Throughput Screening of Promising Redox-Active Molecules with MolGAT". In: *ACS Omega* 8.27 (2023), pp. 24268–24278. URL: https://doi.org/10.1021/acsomega.3c01295.

[115] Mengyao Yu, Yundian Zeng, Mingyang Wang, Chenqing Hua, Sunliang Cui, Peichen Pan, Chang-Yu Hsieh, Tingjun Hou, Odin Zhang, Yufei Huang, Shicheng Chen, Xujun Zhang, Haitao Lin, Zhenxing Wu, Huifeng Zhao, Zaixi Zhang, and Yu Kang. "FragGen: Towards 3D Geometry Reliable Fragment-based Molecular Generation". In: *Chemical Science* (2024), pp. -. URL: http://doi.org/10.1039/D4SC04620J.

[116] Gihan Panapitiya, Peiyuan Gao, C. Mark Maupin, and Emily G. Saldanha. "FragNet: A Graph Neural Network for Molecular Property Prediction with Four Layers of Interpretability". In: *arXiv* (2024), p. 2410.12156. URL: https://doi.org/10.48550/arXiv.2410.12156.

[117] Kha-Dinh Luong and Ambuj K Singh. "Fragment-based Pretraining and Finetuning on Molecular Graphs". In: *Advances in Neural Information Processing Systems*. Ed. by A. Oh, T. Naumann, A. Globerson, K. Saenko, M. Hardt, and S. Levine. Vol. 36. Curran Associates, Inc., 2023, pp. 17584–17601. URL: https://proceedings.neurips.cc/paper_files/paper/2023/file/38ec60a949c3538e5cbb337b1b386dcf-Paper-Conference.pdf.

[118] Guy Bar-Shalom, Beatrice Bevilacqua, and Haggai Maron. "Subgraphormer: Unifying Subgraph GNNs and Graph Transformers via Graph Products". In: *arXiv* (2024), p. 2402.08450. URL: https://doi.org/10.48550/arXiv.2402.08450.

[119] Zuoyu Yan, Junru Zhou, Liangcai Gao, Zhi Tang, and Muhan Zhang. "An Efficient Subgraph GNN with Provable Substructure Counting Power". In: *Proceedings of the 30th ACM SIGKDD Conference on Knowledge Discovery and Data Mining*. KDD '24. Association for Computing Machinery, 2024, pp. 3702–3713. URL: https://doi.org/10.1145/3637528.3671731.

[120] Joseph P. Heindel, Kristina M. Herman, and Sotiris S. Xantheas. "Many-Body Effects in Aqueous Systems: Synergies Between Interaction Analysis Techniques and Force Field Development". In: *Annual Review of Physical Chemistry* 74 (2023), pp. 337–360. URL: https://doi.org/10.1146/annurev-physchem-062422-023532.

A Appendix

A.1 Source Codes and Results

Online Repository We uploaded all source codes and data sets associated with our FBGNN-MBE models, along with their results to the online repositories on Google Drive `https://drive.google.com/drive/u/1/folders/1ZY1EUURG4hD80MgXuxkp7Q0-aaZZ4MtI` and on GitHub `https://github.com/Lin-Group-at-UMass/FBGNN-MBE`.

Pseudo-Algorithms To make sure the readers can reproduce our MXMNet-MBE and PAMNet-MBE models, we provided their protocols as the following pseudo-algorithms.

Algorithm 1: MXMNet-MBE

Input: Molecule data, including atom types, geometries (3D coordinates), and energies (1B, 2B, 3B) derived from MBE
Output: Predicted 2B and 3B energies
Step 1: Initialize embeddings and compute geometric features
$h \Rightarrow \text{initialize\_node\_embeddings}(x)$
$(\text{edge\_index}_g, \text{dist}_g) \Rightarrow \text{radius}(\text{pos}, \text{cutoff}_g)$
$(\text{edge\_index}_l, \text{dist}_l) \Rightarrow \text{remove\_self\_loops}(\text{edge\_index})$
$\text{idx\_angles} \Rightarrow \text{compute\_angle\_indices}(\text{edge\_index}_l)$
Step 2: Encode geometric information
$\text{rbf}_g \Rightarrow \text{BesselBasis}(\text{dist}_g)$
$\text{rbf}_l \Rightarrow \text{BesselBasis}(\text{dist}_l)$
$\text{angle}_1 \Rightarrow \text{compute\_angles}(\text{pos}, \text{idx\_angles.two\_hop})$
$\text{angle}_2 \Rightarrow \text{compute\_angles}(\text{pos}, \text{idx\_angles.one\_hop})$
$\text{sbf}_1 \Rightarrow \text{SphericalBasis}(\text{dist}_l, \text{angle}_1)$
$\text{sbf}_2 \Rightarrow \text{SphericalBasis}(\text{dist}_l, \text{angle}_2)$
Step 3: Message passing layers
$\text{node\_sum} \Rightarrow 0$
for $l \Rightarrow 1$ **to** n_layers **do**
  Global message passing
  $h \Rightarrow \text{GlobalMP}(h, \text{rbf}_g, \text{edge\_index}_g)$
  Local message passing
  $(h, t) \Rightarrow \text{LocalMP}(h, \text{rbf}_l, \text{sbf}_1, \text{sbf}_2, \text{idx\_angles})$
  $\text{node\_sum} \Rightarrow \text{node\_sum} + t$
end
Step 4: Global pooling and prediction output $\Rightarrow \text{global\_add\_pool}(\text{node\_sum}, \text{batch})$
return *output*

Algorithm 2: PAMNet-MBE

Input: Molecule data, including atom types, geometries (3D coordinates), and energies (1B, 2B, 3B) derived from MBE
Output: Predicted 2B and 3B energies
Step 1: Initialize embeddings and compute geometric features
$h \Rightarrow$ initialize_node_embeddings(x)
$(\text{edge\_index}_g, \text{dist}_g) \Rightarrow \text{radius}(\text{pos}, \text{cutoff}_g)$
$(\text{edge\_index}_l, \text{dist}_l) \Rightarrow$ remove_self_loops(edge_index)
idx_angles $\Rightarrow$ compute_angle_indices(edge_index_l)
Step 2: Encode geometric information
$\text{rbf}_g \Rightarrow \text{BesselBasis}(\text{dist}_g)$
$\text{rbf}_l \Rightarrow \text{BesselBasis}(\text{dist}_l)$
$\text{angle}_1 \Rightarrow$ compute_angles(pos, idx_angles.two_hop)
$\text{angle}_2 \Rightarrow$ compute_angles(pos, idx_angles.one_hop)
$\text{sbf}_1 \Rightarrow \text{SphericalBasis}(\text{dist}_l, \text{angle}_1)$
$\text{sbf}_2 \Rightarrow \text{SphericalBasis}(\text{dist}_l, \text{angle}_2)$
Step 3: Message passing with attention
out_global $\Rightarrow$ [], out_local $\Rightarrow$ []
att_global $\Rightarrow$ [], att_local $\Rightarrow$ []
for $l \Rightarrow 1$ **to** n_layers **do**
  Global message passing
  $(h, \text{out}_g, \text{att}_g) \Rightarrow \text{GlobalMP}(h, \text{rbf}_g, \text{edge\_index}_g)$
  Append out_g to out_global
  Append att_g to att_global
  Local message passing
  $(h, \text{out}_l, \text{att}_l) \Rightarrow \text{LocalMP}(h, \text{rbf}_l, \text{sbf}_2, \text{sbf}_1, \text{idx\_angles})$
  Append out_l to out_local
  Append att_l to att_local
end
Step 4: Feature fusion with attention
att_scores $\Rightarrow$ concat(att_global, att_local)
att_weights $\Rightarrow$ softmax(LeakyReLU(att_scores))
out $\Rightarrow$ concat(out_global, out_local)
out $\Rightarrow$ (out $\cdot$ att_weights).sum()
Step 5: Final pooling and prediction
output $\Rightarrow$ global_pool(out, batch)
return *output*

A.2 Fragmentation Strategies

At the current development stage of FBGNN-MBE, the fragmentation strategy was determined case-by-case and depended on the chemical properties the systems in question. We currently focused on the total ground state energy of a system and will investigate the excited state energy soon. We have so far implemented a "top-down" fragmentation strategy with two principles: (1) We maintain the smallest functionally meaningful unit. (2) We break only single bonds or non-bonding interactions [102].

In the present proof-of-concept work we studied water aggregates, phenol aggregates, and water–phenol mixtures. In these systems every single molecule was a natural fragment and an intermolecular interaction like hydrogen bond and van der Waals force plays an essential role in n-body energies ($n \geq 2$). For our future studies about organic polymers, we have tentatively planned to extend the fragmentation strategy by treating each monomer as a fragment, cleaving the carbon–carbon (C−C) bonds, and considering each solvent molecule as a fragment too (if any). We will try our best not to break any complete functional groups like phenyl ($-C_6H_5$) and carboxylic acid ($-$COOH) or known unit like an amino acid and a DNA base.

For a new system, we will run a low-level first-principles MBE_2 calculation where the total energy is truncated at the two-fragment interactions to make sure the fragmentation does not introduce huge estimated error to damage the chemistry. In this way the system will maintain the smallest functional

or repeating unit such as a full π-conjugation, and our model can capture short-range and long-range interactions to simulate the real chemical systems, such as covalent bonds, ionic bonds, hydrogen bonds, London dispersions, dipole–dipole interactions, π–π stacking, and solvation effects.

If a system does not exhibit natural or obvious fragments, such as polyacetylene and polytethlyene, we will consider an alternative "bottom-up" strategy, where we will construct fragments from individual atoms, functional groups, or monomers until some convergence is reached using a low-level first-principles MBE_2 calculation. In this way we will allow fragments to grow around each unit and accommodate underlying effects from local electronic environment and molecular conformations.

We foresaw great room for us to explore and validate our fragmentation strategies and enhance our model versatility and accuracy. However, due to the time constraints, we were unfortunately not able to perform a systematic discussion in the present study. We did validate our top-down fragmentation strategy using a series of water clusters $(H_2O)_n$ (n = 7, 10, 13, 16, and 21) by showing first-principles MP2-MBE_2 and MP2-MBE_3 results in Table 5 in Section A.5. When we treated each water molecule as a single fragment, we reached an average of 3.00% and 0.39% relative errors for these water clusters using MP2-MBE_2 and MP2-MBE_3, confirming a favorable choice of fragmentation strategy.

A.3 Sensitivity Analysis

Number of Layers N_{layer} had a significant impact on the capacity of a GNN model in capturing chemical features [103] and its optimal value was data set-dependent. Our analysis found that increasing N_{layer} from 2 to 4 improved the values of R^2 and MAE for MXMNet-MBE and PAMNet-MBE, indicating a better fit to the training data. However, setting $N_{\text{layer}} = 6$ usually led to marginally diminishing returns with a slight decrease in R^2 and a slight increase in MAE, suggesting possible overfittings (Figure 5. This result supported recent findings that while a deeper GNN architecture can enhance model performance it did not always yield better generalization particularly in molecular property prediction tasks due to overfittings [104].

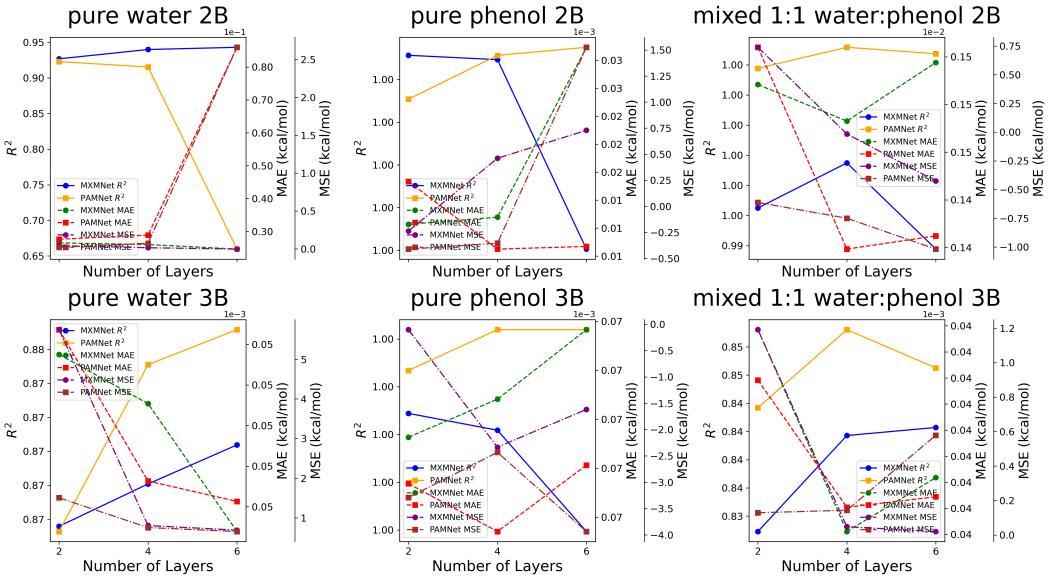

Figure 5: Effects of N_{layer} values on MXMNet-trained and PAMNet-trained values of R^2 and MAE for all benchmark systems.

Local and Global Cut-Off Distances D_{lc} and D_{gc} controled the range of interatomic, intermolecular, and interfragment interactions considered by our FBGNN-MBE. They were sensitive to the character of the system in question and were also crucial to the model performance. For pure water clusters, D_{lc} = 1.7 Å and D_{gc} = 5.0 Å provided optimal results for 3B interactions. These values confirmed that the short-range oxygen–hydrogen bond (O−H, length 0.96Å [105]) and hydrogen bonds (O−H$\cdots$O, length 2.5 to 4.0 Å [106, 107]) dominate the water clusters. For

example, MXMNet-MBE reached $R^2 = 0.9400$ and MAE $= 0.2604$ kcal/mol. For pure phenol clusters, these two values became 3 to 5 Å and 15 Å to effectively capture the long-range van der Waals interactions. For water-phenol mixtures, intermediate cutoff values balanced the short-range and long-range interactions. This result suggested that for a system with medium interfragment interactions like hydrogen bonds, capturing moderate-range interactions provided the best balance between incorporating essential chemical information that can be missed by a smaller cut-off distance and avoiding overfitting due to a larger cut-off distance [108].

Number of Batches N_{batch} emerged as a key factor affecting model performance. Smaller values of N_{batch} like 64 consistently resulted in lower MAE values for both MXMNet-MBE and PAMNet-MBE. This result suggested that smaller batches facilitate more frequent weight updates and allowed the GNN models to fine-tune their parameters more effectively. In contrast, larger values of N_{batch} like 256 or 512 were associated with higher MAE values, likely due to less frequent updates and convergence to suboptimal solutions [109].

Learning Rate k_{learn} also impacted the model performance. A low value of k_{learn} like 0.0001 consistently outperformed higher ones for both MXMNet-MBE and PAMNet-MBE. For example, for the pure water data set, increasing k_{learn} to 0.01 for PAMNet-MBE led to a sharp decline in performance, with R^2 dropping to as low as 0.5981 and a notable increase in MAE to up to 0.9468 kcal/mol. This result confirmed the earlier finding that selecting an appropriate k_{learn} can ensure stable and effective convergence during training [104].

A.4 Mathematical Definition of Evaluation Metrics

Herein we presented the definition of all evaluation metrics used in Table 2 and Figures 3 and 4. We set MP2/DFT evaluated 2B and 3B energies as $\{x_i\}$ and their FBGNN–predicted counterparts as $\{y_i\}$

***R*-Square** R^2 was the coefficient of determination between MP2/DFT and FBGNN-MBE results, defined as

$$R^2 = 1 - \frac{\sum_i (y_i - x_i)^2}{\sum_i \left(y_i - \frac{1}{N} \sum_i y_i \right)^2} \tag{5}$$

Average MP2/DFT result The average result from first-principles (FP) MP2/DFT calculations was defined as

$$\langle E_{\text{FP}} \rangle = \frac{1}{N} \sum_i x_i \tag{6}$$

Mean Signed Error MSE was defined as the average of the signed difference between MP2/DFT and FBGNN-MBE results; as such

$$\text{MSE} = \frac{1}{N} \sum_i (y_i - x_i) \tag{7}$$

Mean Absolute Error MAE was defined as the average of the unsigned difference between DFT/MP2 and FBGNN-MBE results; as such

$$\text{MAE} = \frac{1}{N} \sum_i |y_i - x_i| \tag{8}$$

A.5 Future Applications

Real-Life Systems The ultimate goal of our development of FBGNN-MBE formalisms is to replace QM or QM-MBE methods when an on-the-fly evaluation of FD-PBE is needed for any complex

many-fragment chemical systems. Therefore, it is also worthwhile to validate their capacity in the real-life application scenarios through a systematic assessment of their accuracy, efficiency, and reliability. In the present study in progress, we plan to evaluate the behaviors of MXMNet-MBE and PAMNet-MBE on normal-density water clusters in reproducing three physical properties that can also be generated using MP2 and MP2-PBE, including the total energies of water clusters [$(H_2O)_n$], the one-dimensional (1D) projection of the FD-PES, and the trajectories of MD simulations. These tasks require us to retrain the MXMNet-MBE and PAMNet-MBE using a mixed data set of normal and $2\times$ density clusters. We will select a series of sizes [$(H_2O)_n$] where the size grows from a small isolated molecular complex ($n = 7$) to an actual droplet that solvates the central molecule equally to one in the liquid phase ($n = 21$) [110].

In our preliminary study, we select random water complexes with $n = 7$, 10, 13, 16, and 21 molecules and validate the need of performing MBE even at the MP2 level. Here MP2-MBE$_m$ represents a MP2-based first-principles MBE truncated at the m-body terms, and MXMNet-MBE$_m$ and PAMNet-MBE$_m$ represents FGBNN-based MBE truncated at the m-body terms as discussed in the present study. We summarized the absolute and relative errors for MP2-MBE$_m$ ($m = 1, 2, 3$) using these five random clusters (Table 5), and estimated the upper limits for absolute and relative errors for MXMNet-MBE$_m$ and PAMNet-MBE$_m$ ($m = 2, 3$) by adding the errors of MP2-MBE$_m$ from Table 5 to the MAEs of FBGNN-MBE-generated 2B and/or 3B calculations accumulated from Table 2 (Table 6). We extracted the total CPU times needed for first-principles MP2 (without MBE) using these clusters (Table 7), and estimated the total CPU/GPU times needed for MXMNet-MBE$_m$ and PAMNet-MBE$_m$ ($m = 2, 3$) by adding the accumulated times needed for 1B calculations and the FBGNN-MBE-based 2B and 3B generations.

Table 5: Error Analysis for First-Principles MP2-MBE Using Random Water Clusters

Cluster	Energy	Error					
	MP2	MP2-MBE$_1$		MP2-MBE$_2$		MP2-MBE$_3$	
	hartree	kcal/mol	%	kcal/mol	%	kcal/mol	%
$(H_2O)_7$	−533.92	63.13	0.01884	12.53	0.00374	1.36	0.00041
$(H_2O)_{10}$	−762.77	103.19	0.02156	22.98	0.00480	2.77	0.00058
$(H_2O)_{13}$	−991.61	140.18	0.02253	29.01	0.00466	3.15	0.00051
$(H_2O)_{16}$	−1220.45	180.09	0.02362	38.92	0.00508	4.03	0.00053
$(H_2O)_{21}$	−1601.86	247.90	0.02466	56.20	0.00559	10.87	0.00108

Table 6: Estimated Maximum Error Analysis for FBGNN-MBE$_n$ Using Random Water Clusters

Cluster	Estimated Maximum Error							
	MXMNet-MBE$_2$		PAMNet-MBE$_2$		MXMNet-MBE$_3$		PAMNet-MBE$_3$	
	kcal/mol	%	kcal/mol	%	kcal/mol	%	kcal/mol	%
$(H_2O)_7$	18.00	0.00537	18.38	0.00549	8.10	0.00242	8.31	0.00248
$(H_2O)_{10}$	34.70	0.00725	35.43	0.00740	18.86	0.00394	19.16	0.00400
$(H_2O)_{13}$	49.32	0.00793	50.58	0.00813	33.84	0.00543	34.08	0.00548
$(H_2O)_{16}$	70.17	0.00916	72.11	0.00942	55.61	0.00726	55.53	0.00725
$(H_2O)_{21}$	110.88	0.01103	114.29	0.01137	113.83	0.01132	112.45	0.01119

Table 7: Time Analysis for MP2-MBE$_n$ and Estimated Time Analysis for Random Water Clusters

Cluster	MP2	MXMNet-MBE$_3$	PAMNet-MBE$_3$
	CPU Time	Estimated CPU/GPU Time	
	s	s	s
$(H_2O)_7$	1562.94	9.12	9.05
$(H_2O)_{10}$	18914.93	18.24	17.94
$(H_2O)_{13}$	128084.39	35.73	34.43
$(H_2O)_{16}$	51249.38	62.89	59.69
$(H_2O)_{21}$	121046.76	135.07	125.79

From these results, we can see that the truncation at the 1B terms for water clusters introduce huge relative errors up to 0.025%. (This number appears small but is still too high for a chemical accuracy.)

Inclusion of the 2B and 3B terms significantly enhance the results by reducing the relative errors to up to 0.0056% and 0.0011%, respectively, because an intermolecular interaction, even as weak as van der Waals force or hydrogen bond, play essential roles in chemical properties. This conclusion validates the necessity of applying MBE theory beyond the 1B terms and suggests a truncation at 3B terms or higher. Due to the differences between MP2-MBE and FBGNN-MBE for these water clusters, the estimated maximum errors of FBGNN-MBE are larger than MP2-MBE but still acceptable, all below 0.011%. In addition, our FBGNN-MBE calculations can reduce the computational cost by at least three orders of magnitude for water clusters compared to single-shot MP2 calculations for the whole clusters. These two pieces of findings, although made based on estimated errors and computational costs, tentatively validates the efficiency and accuracy of FBGNN-MBE methods.

Planned Comparison with Other Conventional GNN Models In the near future, we will make a more complete assessment of the model performance of FBGNN-MBE by comparing with latest advanced fragment-based NN or GNN models designed for molecular properties, such as SE3Set [111], MACE [112], MGSSL [113], MolGAT [114], FragGen [115], FragNet [116], GraphFP [117], Subgraphormer [118], and ESC-GNN [119].

Utility in Molecular Dynamics In the present set up, we approximated the first-principles FD-PESs, or in other words, geometry-dependent electronic energies under the Born–Oppenheimer approximation at $T = 0$ K, using FBGNN-MBE-generated counterparts. We can evaluate all relevant forces as the gradients of these potential energies [98, 120]. In this way, we expected to replace a first-principles FD-PES with a FBGNN-MBE-generated FD-PES in *ab initio* molecular dynamics (AIMD). Because of this equivalent substitution, the obedience or violations to some underlying rules for FGBNN-MBE-generated forces, such as energy conservation, will depend on the overall set up of the AIMD simulation. If the AIMD simulation is set up at constant NVE (microcanonical ensemble), the energy will be conserved. However, if AIMD simulation is set up at constant NVT (canonical ensemble) or μVT (grand canonical ensemble), the temperature remains a constant through a computational thermostat but the energy will no longer be conserved.